Simple models of complex aggregation: Vesicle formation by soft repulsive spheres with dipolelike interactions

P. Ballone and M. G. Del Pópolo
Atomistic Simulation Centre, School of Mathematics and Physics, Queen's University, Belfast BT7 1NN, United Kingdom
(Received 14 December 2005; published 14 March 2006)

Structural and thermodynamic properties of spherical particles carrying classical spins are investigated by Monte Carlo simulations. The potential energy is the sum of short range, purely repulsive pair contributions, and spin-spin interactions. These last are of the dipole-dipole form, with however, a crucial change of sign. At low density and high temperature the system is a homogeneous fluid of weakly interacting particles and short range spin correlations. With decreasing temperature particles condense into an equilibrium population of free floating vesicles. The comparison with the electrostatic case, giving rise to predominantly one-dimensional aggregates under similar conditions, is discussed. In both cases condensation is a continuous transformation, provided the isotropic part of the interatomic potential is purely repulsive. At low temperature the model allows us to investigate thermal and mechanical properties of membranes. At intermediate temperatures it provides a simple model to investigate equilibrium polymerization in a system giving rise to predominantly two-dimensional aggregates.

DOI: 10.1103/PhysRevE.73.031404 PACS number(s): 82.70.Uv, 87.16.Dg, 68.65.−k, 81.16.Dn

I. INTRODUCTION

Particles interacting with angle-dependent potentials challenge the common belief that well behaved substances limit themselves to a few homogeneous phases, usually consisting of a crystal and a fluid phase, this last differentiating into liquid and gas over a limited range of thermodynamic conditions. Spherical particles carrying a classical electrostatic dipole, in particular, provide perhaps the most apparent example of how a complex behavior can arise even from fairly basic ingredients [1,2]. Although the full phase diagram of this system is still the subject of some debate [3–5], it is generally accepted that at low density and temperature dipolar spheres give rise to predominantly one-dimensional (1D) aggregates [6,7].

We show that a simple change of sign for the dipole-dipole energy gives rise to an interaction potential whose low density, low temperature phase diagram includes equilibrium assemblies of free-floating vesicles. Each vesicle has a simple spin arrangement, whose stabilization with decreasing temperature provides the driving force for condensation, and determines the shape and size of the resulting aggregates. In what follows we shall refer to the modified model as antidipoles, to emphasize the sign change with respect to the electrostatic case.

The model, first of all, represents an additional playground to test existing liquid state theories, and provides fresh motivations to develop new ones, especially for long range, angular-dependent interactions [8]. Of particular interest is the interrelation of density and spin transitions taking place at condensation [9]. Moreover, particle models with effective interactions are increasingly used as a coarse grain approximation for complex systems [10]. Thus, dipolar soft spheres have often been proposed as prototypes of equilibrium polymerization [11], attributing to each particle the role of a monomer finding its way into dynamically defined 1D aggregates. Antidipoles, giving rise to vesicles, provide a different example of aggregation, starting from a homogeneous fluid, ending up into predominantly two-dimensional (2D) structures embedded into the usual three-dimensional (3D) space. As such, the present model may provide results complementing the picture provided by dipoles, highlighting the role of dimensionality and long range interactions in the condensation process. Preliminary investigations with a shorter range version of the antidipole model show qualitatively different features in the phase diagram, underlining the richness of structures and phase behavior of systems with angular-dependent forces.

Perhaps more importantly, coarse graining models based on particles are being used to investigate self-assembling structures of interest for nanotechnologies and for biology [12]. Then, antidipoles provide a simple way to investigate thermal and mechanical properties of membranes [13], including organic and biological ones. In this respect, our potential is a member of the family of solvent-free models for amphiphilic systems described in Ref. [14] of which antidipoles are arguably the simplest example. The idealized form of the potential, in turn, makes our model particularly suitable to investigate large scale properties of amphiphile systems, not closely dependent on the atomistic details of the constituent molecules [15].

Needless to say, the direct interaction of amphiphile molecules, which could be computed by standard force fields, is not expected to resemble the antidipole pair potential. Their interaction in solution, however, is much more difficult to characterize, and, to the best of our knowledge, it is still largely unknown. Then, the qualitative similarity of equilibrium structures in our simulations and in experiment might suggest that the antidipole potential does indeed capture some essential features of the true effective interaction.

II. THE MODEL AND THE SIMULATION METHOD

The system is made by N soft repulsive particles at positions $\{\mathbf{r_i}, i=1,\ldots,N\}$, each carrying a vector

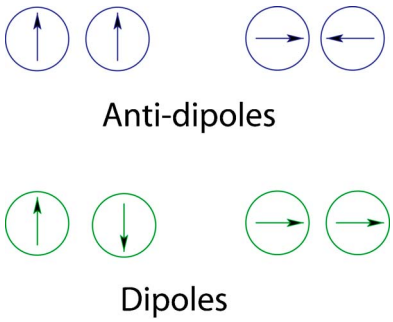

FIG. 1. (Color online) Lowest energy configurations for dipoles and antidipoles.

$\{\mathbf{S_i}, i=1,\ldots,N\}$ of fixed length S and variable orientation. The system potential energy is

$$U_{ADip}(\mathbf{r_1},\ldots,\mathbf{r_N}|\mathbf{S_1},\ldots,\mathbf{S_N}) = \frac{1}{2}\sum_{i\neq j}\epsilon\left\{4\left(\frac{\sigma}{|\mathbf{r_{ij}}|}\right)^{12} - \sigma^3\left[\frac{\mathbf{S_i}\cdot\mathbf{S_j}}{|\mathbf{r_{ij}}|^3} - \frac{3(\mathbf{S_i}\cdot\mathbf{r_{ij}})(\mathbf{S_j}\cdot\mathbf{r_{ij}})}{|\mathbf{r_{ij}}|^5}\right]\right\}, \quad (1)$$

where $\mathbf{r_{ij}}=\mathbf{r_i}-\mathbf{r_j}$, and $(\sigma,\ \epsilon)$ provide natural length and energy scales ($\sigma=\epsilon=1$), respectively. Both the $\mathbf{S_i}$ vectors and their common norm S are dimensionless. Particles are enclosed in a cubic box of side L, with periodic boundary conditions (pbc) implied. Interparticle interactions are computed within the minimum image convention, i.e., the sum of Eq. (1) includes all and every pair whose separation is less than $L/2$ along each of the Cartesian coordinates, considering also periodic images. With the system sizes considered in our simulations ($20\leqslant L/\sigma\leqslant 40$) the minimum image convention is more than adequate for the isotropic part of the potential (decaying like r^{-12}), but it remains questionable for the long range, spin part. However, the error introduced by our approximate treatment of pbc has been estimated by simple analytic approximations, and found to be negligible for the system sizes ($N\geqslant 1200$), densities ($\rho=N/L^3\leqslant 0.15$) and spin correlations (predominantly 2D, with negligible 3D average polarization) of interest for the present study.

Simulations are performed by Monte Carlo (MC) in the canonical (NVT) ensemble, aiming at inhomogeneous (two phases) conditions at low density and low temperature. Single moves attempt to change either the position of the individual particles, or the orientation of their $\mathbf{S}$ vector.

The spin-dependent part of the interparticle potential in Eq. (1) is apparently modeled on the interaction between two electrostatic dipoles, with however, a crucial change of sign. As a result, the angular pattern of attractive and repulsive interactions is interchanged (see Fig. 1). The model can be thought of as arising from a modified electrostatic field, in which charges of the same sign do attract each other, and unlike charges repel each other. Charge segregation is prevented by the fact that positive and negative charges are rigidly bound in dipoles.

Comparisons are made with the well known dipolar soft spheres, whose potential energy is

$$U_{Dip}(\mathbf{r_1},\ldots,\mathbf{r_N}|\mathbf{P_1},\ldots,\mathbf{P_N}) = \frac{1}{2}\sum_{i\neq j}\epsilon\left\{4\left(\frac{\sigma}{|\mathbf{r_{ij}}|}\right)^{12} + \sigma^3\left[\frac{\mathbf{P_i}\cdot\mathbf{P_j}}{|\mathbf{r_{ij}}|^3} - \frac{3(\mathbf{P_i}\cdot\mathbf{r_{ij}})(\mathbf{P_j}\cdot\mathbf{r_{ij}})}{|\mathbf{r_{ij}}|^5}\right]\right\}. \quad (2)$$

The vectors $\{\mathbf{P_i}, i=1,\ldots,N\}$ play a role similar to that of S, and a different name is selected in order to emphasize the different interaction in the two cases.

A few test computations have been performed with a finite range version of the antidipole model, obtained by multiplying each pair contribution by a smoothed step function $f(r)$, defined as follows: $f(r)=1$ for $r\leqslant R_c$; $f(r)=0$ for $r\geqslant(R_c+\Delta)$, and $f(r)=\alpha(R_c+\Delta-r)^2+\beta(R_c+\Delta-r)^3$ for $R_c<r<R_c+\Delta$. The parameters R_c and Δ specify the range of the potential $(R_c+\Delta/2)$ and the width of the smoothing region (Δ). The α and β coefficients are selected in such a way that $f(r)$ and $df(r)/dr$ are continuous everywhere.

III. SIMULATION RESULTS

Most computations have been done for systems of 9600 particles, exploring a wide temperature range and focusing on low density conditions ($\rho\sigma^3=0.15$) leading to a two-phases configuration at low T. The relative strength of short-range and spin-spin interactions has been tuned by setting $S=|\mathbf{S}|=2$. Test computations, and all the simulations involving true electrostatic dipoles, have been performed with a smaller system made of $N=1200$ particles.

In a first stage, we carried out a simulated annealing for a sample of $N=9600$ particles, starting from a temperature ($T=1.8$) such that the system is apparently homogeneous and fluid. Temperature has been reduced down to $T=0$ in regular steps of amplitude $\delta T=0.1$. Each temperature variation has been followed by an equilibration stage of 1200 MC steps/particle. This minimal block of equilibration steps has been repeated (up to six times for $T=1.2$) whenever running averages of thermodynamic quantities displayed a visible drift during the 1200 MC steps/particle run. Following equilibration, the statistical properties discussed below have been computed during a production run of 1200 MC steps/particle. The full annealing cycle from $T=1.8$ to $T=0$ has been repeated two times. The average quantities discussed below are all averaged also on the two independent annealings.

A longer annealing cycle (by roughly a factor of ten) for the $N=1200$ sample gave results very close to those obtained for the $N=9600$ particles sample, with expected differences for the quantities (like the size distribution of aggregates, see below) most sensitive to finite size and short time errors. Despite the satisfactory outcome of this test, we cannot exclude a residual dependence of the results on size and on annealing rate, since long-lived metastable configurations and kinetic effects are far more important for systems with anisotropic interactions and configurations made of disjoint clusters than for homogeneous systems with isotropic potentials. In the case of amphiphilic systems, this sensitivity on size and time scales extends far beyond the reach of simulation, affecting even the results of laboratory experiments tak-

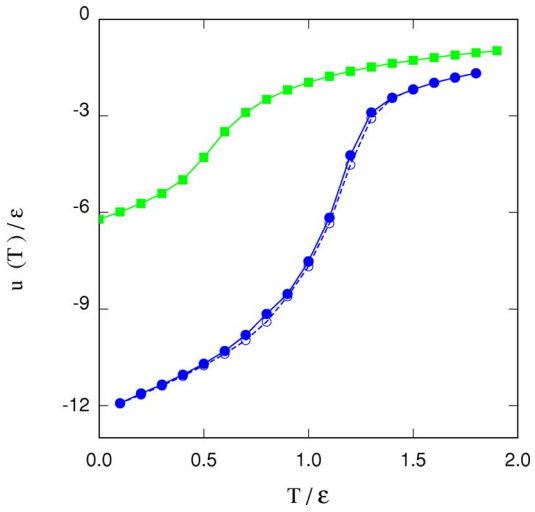

FIG. 2. (Color online) Average potential energy per particle as a function of temperature computed on cooling (filled dots) and on heating (open circles) a sample of $N=9600$ antidipoles. The results for a smaller ($N=1200$) sample of dipolar spheres on cooling are shown for comparison (filled squares). Lines are a guide to the eye. Error bars are comparable to the symbols size.

ing place on macroscopic times and lengths [16].

The evolution of the $N=9600$ particle system with decreasing temperature T has been monitored by computing thermodynamic properties, and by inspection of snapshots. The average potential energy per particle u as a function of T is shown in Fig. 2. The results for particles carrying electrostatic dipoles are reported on the same figure for comparison [17]. At $T>1.3$, u depends only weakly on temperature. Decreasing temperature down to $T=1.3$ triggers a condensation process as apparent from a drop of the potential energy and from snapshots, showing the formation of persistent density fluctuations. At $T=1.2$ these last give rise to aggregates of up to a few hundred particles, whose structure is highly disordered at first, but becomes increasingly recognizable with a further decrease of temperature. At $T\leqslant 1.1$ the system is made of a population of free-floating vesicles, i.e., hollow aggregates in which particles are regularly distributed on a rounded, finite surface closing onto itself (see Fig. 3). The size of these aggregates corresponds to those of the persistent density fluctuations described above, i.e., they extend up to several hundred particles. At $T=1.1$ vesicles are immersed into a dilute vapor of single particles and other very small fragments.

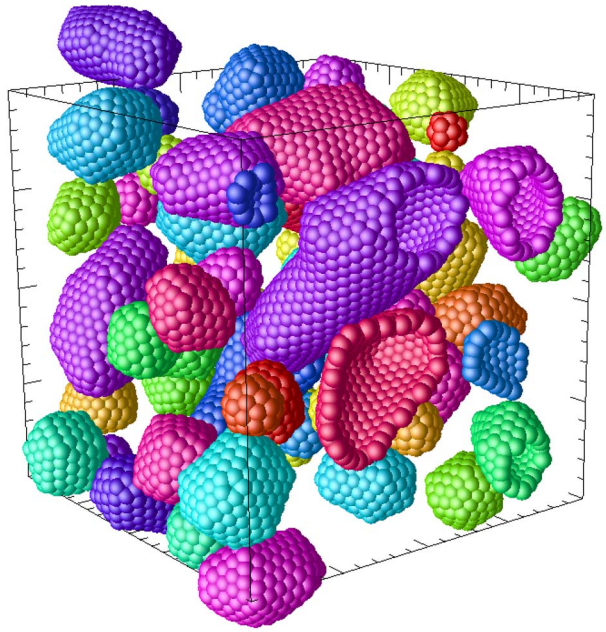

FIG. 3. (Color online) Lowest energy ($T=0$) configuration found by simulated annealing for a sample of $N=9600$ antidipoles. The system has been cut along a plane parallel to one side of the simulation cell to show that aggregates are hollow.

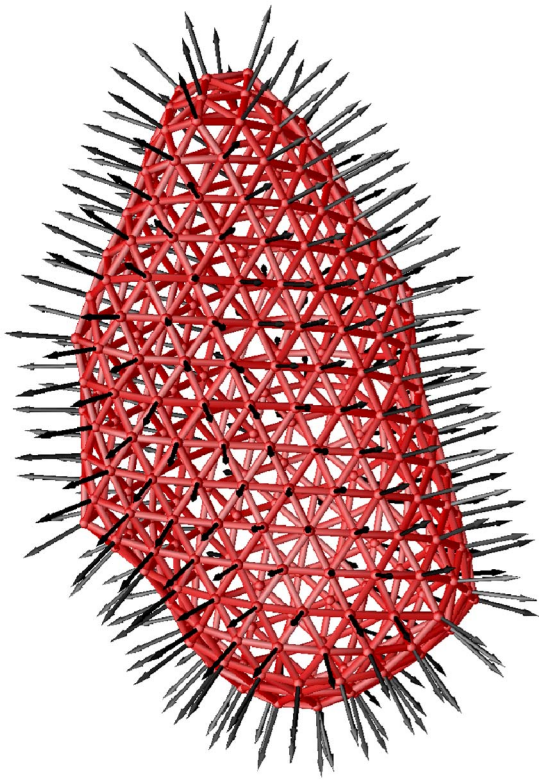

FIG. 4. (Color online) Snapshot of a single o-vesicle at $T=0$. Vectors give the direction of the spins carried by each of the 320 particles in the vesicle.

The aggregation process is apparently driven by the stabilization of a well defined spin pattern, since attractive spin-spin interactions are the only possible source of cohesion for otherwise purely repulsive spheres. Snapshots confirm that already at $T=1.1$ spins display a strong degree of order, with all the spins of each vesicle pointing either outwards ("o-vesicles") or inwards ("i-vesicles") (see Fig. 4). The inward and outward spin configurations are degenerate for individual vesicles, but their relative orientation determines the sign of the weak residual interaction among vesicles. Comparison of the system potential energy with the cohesive energy of isolated aggregates shows that in our simulated samples the vesicle-vesicle interaction energy is positive and quantitatively very small.

The phase transformation described above is reflected in the temperature dependence of the system correlation func-

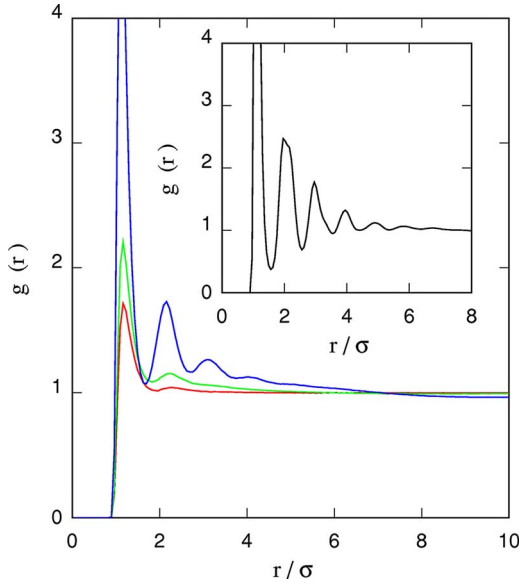

FIG. 5. (Color online) Radial distribution function of antidipoles. In order of increasing coordination, the curves refer to $T=1.5$, $T=1.3$, and $T=1.1$. The radial distribution function at the onset of solidlike order ($T=0.7$) is shown in the inset.

tions. At $T>1.5$, for instance, the particle-particle radial distribution function $g(r)$ displays only a modest and narrow peak at $r/\sigma=1.16$, followed by a structureless tail at longer distances (see Fig. 5). The aggregation process taking place around $T=1.2$ is accompanied by an increase in the height of the first peak of $g(r)$, and by the progressive appearance of further correlation peaks. The stabilization of the long wavelength ($\Lambda \approx 10\sigma$) density fluctuations giving rise to different vesicles is reflected in the behavior of the radial distribution function at distances $10 \leqslant r/\sigma \leqslant 15$, deviating significantly $[g(r) \approx 0.98]$ from the asymptotic value $[g(r)=1]$ of homogeneous systems. These features, characteristic of strongly correlated, inhomogeneous systems, become progressively more apparent with decreasing temperature down to $T=0.7$. At this last temperature, the second peak of $g(r)$ splits into two, while further peaks become asymmetric and display a fine structure pointing to the formation of a solidlike (or perhaps a glasslike) ordering of particles within each vesicle [18]. This observation suggests that vesicles are liquidlike in the temperature range $0.7<T \leqslant 1.2$. The local structure of low temperature vesicles is predominantly hexagonal, with distortions and defects (discussed in more detail below) required to cover the rounded but somewhat irregular shapes of the vesicles. Careful energy optimization at $T=0$ results in a modest but still apparent degree of faceting of the vesicles' surface, giving rise to fairly large and nearly flat domains joined at rounded edges.

The phase behavior along the $\rho=0.15$ line for $0 \leqslant T \leqslant 1.8$ is summarized by the plot of the constant volume specific heat [19] $c_v(T)=du(T)/dT$. As shown in Fig. 6, $c_v(T)$ displays a major peak at $T_{cond}=1.2$, marking condensation. This peak is broad and asymmetric. Its wider, low-temperature side partly hides a weak secondary maximum at $T_{order}=0.7$. The precise correspondence of this peak with the qualitative changes in $g(r)$ described above and attributed to

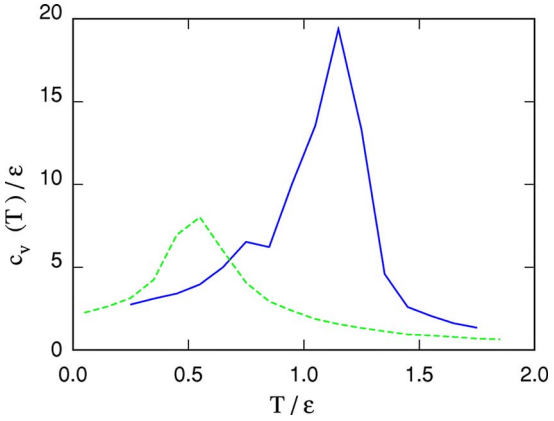

FIG. 6. (Color online) Configurational part of the constant volume specific heat computed by finite difference differentiation of the potential energy per particle $u(T)$. Full curve: antidipoles; dashed curve: electrostatic dipoles.

a liquid-solid transition, reinforces our confidence in the identification of this weak anomaly. These observations confirm that the ordering of particles already incorporated into well defined vesicles takes place through a phase transition, although weakened and severely rounded by the finite size of individual aggregates.

The location of the two maxima at $T_{cond}=1.2$ and $T_{order}=0.7$ provides our best estimate for the corresponding transition temperatures. The identification of the corresponding transition order, or, at least, a precise statement on their continuous or discontinuous character would require much longer computations, and a careful analysis of the size scaling behavior. The preliminary evidence provided by our simulations suggests that both transitions are continuous, or, at most, very weakly discontinuous. This conclusion is supported by the results of a reverse thermal cycle, in which the temperature of the $T=0$ sample is increased up to $T=1.8$, following a schedule reproducing in reverse the cooling progression. The $u(T)$ obtained on heating closely follows the cooling energy curve, showing that the two transformations occur with negligible or no hysteresis. Somewhat surprisingly, the only uncertain signs of discontinuity and hysteresis are found for the weakest of the two transitions, i.e., at $T=0.7$, but the accuracy of our data is not sufficient to reach a firm conclusion.

Condensation, therefore, appears to be similar to the corresponding continuous phase change observed for electrostatic dipoles, while the liquidlike to solidlike transition seen in antidipoles has no counterpart for dipoles.

The spin-spin correlation function, defined as follows:

$$4\pi\rho\frac{S^2}{3}r^2 g_{SS}(r) = \frac{1}{N}\left\langle \sum_{i\neq j}^{N} \mathbf{S_i}\cdot\mathbf{S_j}\delta(|\mathbf{r_i}-\mathbf{r_j}|-r)\right\rangle \qquad (3)$$

provides a picture of condensation and then solidification completely analogous to the one given by $g(r)$.

In principle, also the information provided by the structure factor and its spin-spin version is strictly equivalent to that given by $g(r)$. Nevertheless, the particle-particle struc-

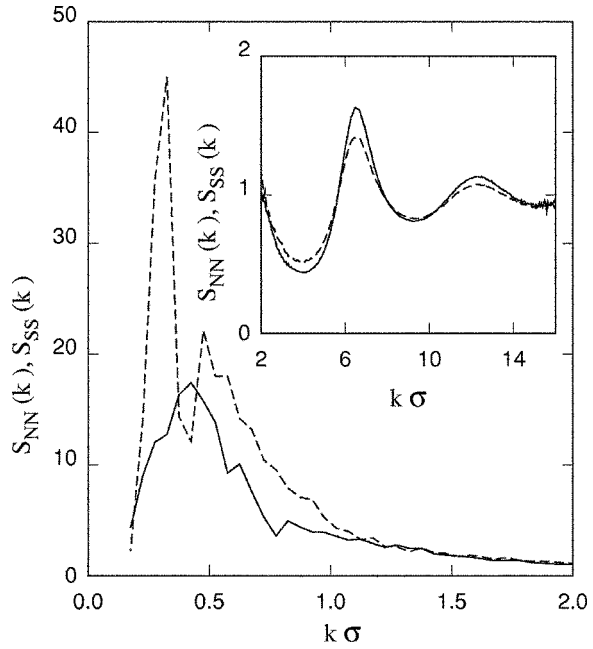

FIG. 7. Long wavelength portion ($k \leqslant 2$) of the particle-particle [$S_{NN}(k)$, full line] and spin-spin [$S_{SS}(k)$, dash line] structure factors of antidipoles at $T=1$, $\rho=0.15$. The inset shows these same two functions on an extended k range. The relative error bar is 10% for $k \leqslant 0.6$, and $\sim 1\%$ for $k \sim 2\pi/\sigma$.

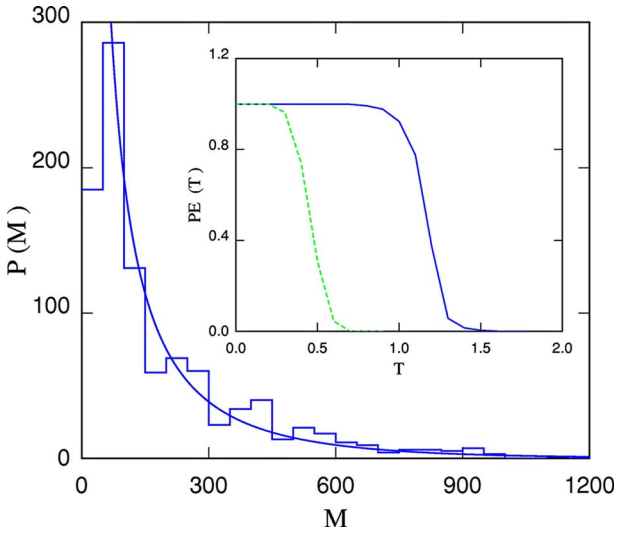

FIG. 8. (Color online) Size distribution probability $P(M)$ of antidipole vesicles as a function of cluster size M at $T=0.9$. Histogram: simulation results. The continuous line is an interpolation based on the Schulz function $P(M)=A \exp(-0.0025M)/M$. The histogram and the interpolation have the same (but otherwise arbitrary) normalization. Relative error bars are of the order of 18%. Inset: Extent of polymerization PE as a function of temperature. Aggregates belong to the polymerized fraction if their size exceeds $M=12$. Full line: antidipoles; dashed line: electrostatic dipoles.

ture factor $S_{NN}(k)$ and its spin-spin counterpart $S_{SS}(k)$ [related to $g_{SS}(r)$ by the same transformation linking $S_{NN}(k)$ to $g(r)$] provide a remarkable view of the system evolution, and for this reason they are briefly discussed here. First of all, over the entire temperature range explored in the present study the highest peak of both $S_{NN}(k)$ and $S_{SS}(k)$ is located at $k_{max}\sigma \sim 0.4$, while in most simple liquids far from their critical point the main peak of $S(k)$ is found at $k_{max}\sigma \sim 2\pi$, reflecting the size of the short range correlation hole. The high value of $S_{NN}(k)$ and $S_{SS}(k)$ at low k and high temperature ($T>1.3$) unambiguously points to an incipient instability of the homogeneous fluid phase with respect to long wavelength density fluctuations. Moreover, the comparison of $S_{NN}(k)$ and $S_{SS}(k)$ in the condensed phase ($T \leqslant 1.3$), reveals expected similarities, but also a few interesting differences. As shown in Fig. 7, The low-k peak of S_{SS} at $T=1$ is clearly asymmetric. It reaches its highest value at $k\sigma \sim 0.3$, it goes through a dip at $k\sigma \sim 0.4$ before rising to a secondary maximum at $k\sigma=0.5$, and then it decays slowly at higher k's. By contrast, the peak of S_{NN} is more symmetric and narrower, reaching its highest value at $k\sigma \sim 0.4$, i.e., where S_{SS} presents its characteristic dip. The wider and more structured S_{SS} peak is apparently related to the coherent ordering of the spins spanning the entire surface of each aggregate, which includes a full 2π turn of the spin direction along every path circling the vesicles equatorial line.

As mentioned in the Introduction, the present model provides a useful tool to investigate the statistical mechanics of equilibrium aggregation in systems giving rise to membrane-like structures. In our study, individual aggregates have been identified by dividing particles into *connected* structures, where being connected requires that (i) each particle is within 1.3σ from at least another particle in the cluster, and (ii) every two particles (i,j) separated by less than 1.3σ are connected if and only if their spins satisfy the relations: $\mathbf{S_i}\cdot\mathbf{S_j} \geqslant 0.5S^2$; $|\mathbf{S_i}\cdot\mathbf{r_{ij}}|$ and $|\mathbf{S_j}\cdot\mathbf{r_{ij}}|$ are both $<0.2S|\mathbf{r_{ij}}|$. Requirement (ii) has been introduced to identify as distinct vesicles on occasional collisions, when a few of their particles might approach each other within the cut off distance of 1.3σ. In what follows we shall include in the condensed (or *polymerized*) phase all aggregates whose size is larger than the (arbitrary) lowest value of twelve particles, while smaller aggregates and single particles represent the vapor or unpolymerized fraction. The temperature-dependence for the average value of the polymerized fraction $PE(T)$, usually referred to in the literature as the *polymerization extent*, is represented by a slightly rounded step function (see the inset in Fig. 8), changing from zero to one in a narrow temperature interval around $T_{cond}=1.2$. The sharpness of the transition, together with the strict saturation of $PE(T)$ to its limiting value $PE(T)=1$ for $T \leqslant 0.7$, highlights the remarkable strength of the thermodynamic force driving the system towards polymerization. In this respect, the behavior of antidipoles appears to be analogous to that of electrostatic dipoles, whose $PE(T)$ is also shown in the inset of Fig. 8.

The dilute (unpolymerized) component surrounding vesicles at condensation provides a mechanism to exchange particles and to modify the size of vesicles, thus allowing the system to relax towards an equilibrium distribution of sizes. The density of this dilute component, however, decreases rapidly with decreasing temperature, practically vanishing below $T=0.8$. Vesicles, therefore, behave like isolated entities for $T<0.8$, conserving their particles and size down to the lowest temperature. In what follows, the distribution of

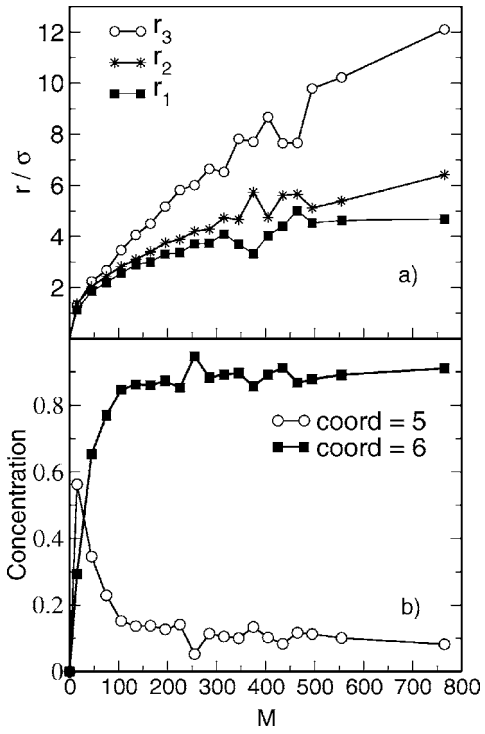

FIG. 9. (a) Average gyration radii r_1, r_2, r_3 (ordered by length) as a function of cluster size M. (b) Concentration of fivefold and sixfold coordinated particles in vesicles of size M.

vesicles for $0.8 \leqslant T \leqslant 1.2$ is taken as representative of equilibrium conditions, while at lower temperatures the results are likely to be affected by kinetic effects. Needless to say the equilibration of cluster sizes is a slow process at all temperatures, since it relies on the particles long range diffusion, and on fairly rare fusion and fragmentation events [20].

The equilibrium size distribution probability $P(M)$ at $T=0.9$ as a function of cluster size M, is shown in Fig. 8. The relative minimum at very low sizes ($M \leqslant 50$) is due to the fact that we exclude aggregates smaller than 12 particles. Above $M \sim 50$, the size distribution, extending up to ~ 1200 particles, is well approximated by $P(M)=A \exp(-\lambda M)/M$, with $\lambda=0.0025$, while A is determined by the normalization imposed on $P(M)$. A distribution of this form (Schulz distribution) agrees with the mean-field predictions for the size distribution of equilibrium polymers in the dilute regime [21], and provides an excellent fit to the simulation data for a variety of other equilibrium polymerization models [22]. The average cluster size is $\langle M \rangle = 198 \pm 20$ at $T=0.9$, and reduces slightly to $\langle M \rangle = 168 \pm 20$ at the end of the annealing ($T=0$).

The equilibrium size distribution $P(M)$ of vesicles and micelles made of amphiphilic molecules has been investigated in the past using computer simulation based on a variety of different models (representative examples are given by Refs. [23–25]). The size distribution probability found by these previous studies is either monotonic, as in our case, or bimodal, peaking at $M \sim 1$ and at $M \sim 50$–100. The qualitative difference in the results is likely to be due to the different models used in the simulation, to the different thermodynamic state, and also to the different thermal history of the simulated samples.

The shape of vesicles has been characterized by finding the principal axes of each aggregate, and computing the corresponding radii. The three radii r_1, r_2, and r_3, listed in order of increasing length, in most cases satisfies the relation: $r_1 \sim r_2 < r_3$, corresponding to prolate spheroids. Moreover, the aspect ratio $Q=2r_3/(r_1+r_2)$ depends mainly on size, allowing us to characterize the shape of vesicles by plotting the average r_1, r_2, and r_3 as a function of M [see Fig. 9(a)]. The results show that small vesicles are nearly spherical, a conclusion confirmed by the analysis of snapshots. Moreover, Q increases slowly but monotonically with increasing size M, suggesting that the limiting form of very large aggregates is a tube. This conclusion is supported by the results of computations for regular particle configurations on simple surfaces (plane, sphere, cylinder, etc.). The lowest energy is found for a compact hexagonal distribution of particles on a cylinder of radius $R_{cyl}=6.6\sigma$, with a nearest neighbor interparticle distance of 1.09σ. The computed energy per particle $u_{cyl}=-12.69\epsilon$ is $\sim 4\%$ lower than the average energy per particle $u_{anneal}=-12.2\epsilon$ at the end of the annealing cycles described above.

The diameter of the largest clusters found in our simulations, consisting of more than 1000 particles, is of the order of $L/2$, and it is conceivable, therefore, that their size and shape is affected by the finite dimension of our samples.

The rounded shape of vesicles results from the optimal combination of distributed curvature and localized defects minimizing the surface free energy. A detailed discussion of topological defects on the surface of vesicles, i.e., disclinations and dislocations, is beyond the scope of the present study. We limit ourselves to the computation of the average concentration of miscoordinated atoms for the annealed ($T=0$) samples, reminding, in passing, that in a planar lattice under- and overcoordinated atoms are associated to (positive and negative) disclinations, and dislocations can be seen as closely bound pairs of disclinations [18]. Here we are implicitly assuming that normal coordination is six, since the ground state structure for antidipoles on a plane is the well known hexagonal lattice.

The coordination of each atom is computed as the number of neighbors within the cutoff distance of 1.3σ. The average coordination of particles, and the concentration of coordination defects depend mainly on the size of the vesicle. This observation, once again, allows us to summarize our results in a plot of the average concentration of n fold coordinated particles as a function of cluster size [see Fig. 9(b)]. It is found that the only miscoordination present at a sizable concentration is five. As expected, fivefold coordinated particles are far more abundant in smaller aggregates, and become increasingly dilute with increasing cluster size. The concentration of sevenfold and fourfold coordinated particles is negligible, although not strictly vanishing, at all sizes.

The compact and regular arrangement of particles at low temperature provides an explicit triangulation of the vesicles surface, which can be exploited to compute local geometrical and mechanical properties. For instance, the bending energy of a membrane of bending rigidity k is given by [13]

$$E_{bend} = \frac{k}{2} \int H^2(R) dA, \tag{4}$$

where $H(R)$ is the local mean curvature

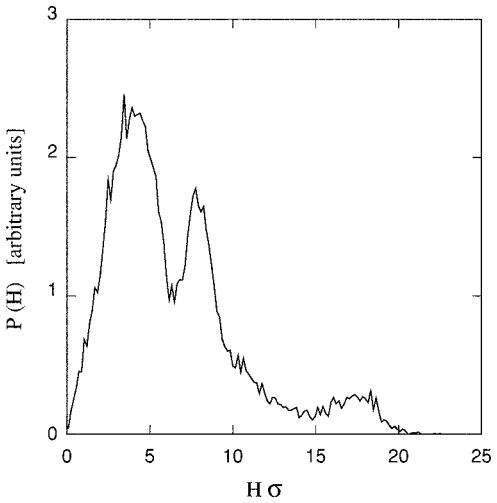

FIG. 10. Probability distribution for the local curvature H_i (see the text) in antidipole vesicles at $T=0$.

$$H(R) = \frac{k_1(R) + k_2(R)}{2}, \tag{5}$$

$k_1(R)$, $k_2(R)$ are the principal curvatures at point R on the surface (see Ref. [26]), and the integral extends over the entire surface. A discretized form of Eq. (4) valid for a triangulated surface is given by [27–29]

$$\tilde{E}_{bend} = \frac{k}{2}\sum_i \frac{1}{\Omega_i}\left[\sum_j (\mathbf{R_j} - \mathbf{R_i})\right]^2, \tag{6}$$

where the first sum extends to all triangulation nodes (i.e., to all particles), the sum in parenthesis extends to the neighbors connected to i by a bond, and Ω_i is the total area of the triangles converging to node i. Comparison of Eqs. (4) and (6) shows that for a regular triangulation the local quantity

$$H_i = \frac{1}{\Omega_i}\sqrt{\left[\sum_j (\mathbf{R_j} - \mathbf{R_i})\right]^2} \tag{7}$$

is directly proportional to the average curvature at node i, in our case coincident with particle i. Visualization of snapshots shows that the definition of Eq. (7) correctly associates high curvature energy to vertices and edges of large vesicles, as well as to all atoms of small aggregates. The probability distribution $P(H)$ at low T displays three distinct peaks (see Fig. 10). The lowest curvature peak ($H \leqslant 6$) accounts for the majority of particles, and corresponds to nearly flat facets of medium and large vesicles. The peak at intermediate curvature ($6 \leqslant H \leqslant 12$) corresponds to particles at vertices and edges, while the high curvature peak ($H > 12$) corresponds to particles belonging to small aggregates.

The bending rigidity k could be computed explicitly by computing the energy of surfaces of known curvature (spheres, cylinders), and thermal averages of $\tilde{E}_{bend}$ provide thermodynamic functions related to the membranelike properties of the vesicles.

The observation of an equilibrium population of finite aggregates with a closed, rounded, 2D geometry raises the problem of what are the forces at play stabilizing this unusual equilibrium configuration. This analysis has to include the anisotropy of cohesive forces, the strength of bending rigidity, and entropy contributions certainly relevant close to the condensation temperature T_{cond}. The peculiar angular dependence of the spin-spin interaction is clearly responsible for the 2D character of vesicles. Bending rigidity and entropy compete in the determination of the size distribution probability; bending energy favors flat terraces and thus large aggregates, while entropy favors small clusters, retaining a portion of the ideal translational entropy lost at condensation.

In addition to these obvious ingredients, a major role in the determination of equilibrium sizes and shapes of the condensed species is played by the range of the spin-spin interactions. Test computations with a short range version of the potential give a surprisingly wide variety of different results. The simulated annealing of a short range model with a cutoff specified by $R_c = 3.5\sigma$, and $\Delta = 0.2\sigma$ (see the last paragraph of Sec. II) results in a compact geometry, whose residual 2D character manifests itself in an apparent layering of the condensed phase, with a strict antiferromagnetic coupling of planes.

An intermediate version of the model, having $R_c = 10\sigma$ and $\Delta = 0.2\sigma$ gives rise again to hollow 2D aggregates, whose size distribution is, however, shifted toward sizes lower than in the long range case. The average cluster size at $T=0$, for instance, is reduced to $\langle M \rangle = 145 \pm 7$, to be compared with $\langle M \rangle = 168 \pm 20$ in the full range case.

IV. SUMMARY AND CONCLUDING REMARKS

A simple change of sign in the dipole-dipole energy of soft, repulsive dipolar spheres results in a qualitatively different model (antidipoles), giving rise at low density and low temperature to an equilibrium population of free-floating vesicles.

The model, first of all, might be valuable as a testing ground for theories of aggregation and equilibrium polymerization in systems with angle-dependent interactions, in many ways complementing the picture provided by dipolar spheres.

Our computations provide a preliminary but broad exploration of the model properties, identifying two phase transitions taking place at constant density as a function of temperature. With decreasing temperature, the first transition takes place at $T_{cond} = 1.2$, and leads from a homogeneous fluid phase to an assembly of predominantly 2D aggregates, consisting of rounded prolate bodies weakly interacting with each other. This transformation is driven by a (simultaneous) transition in the spin-spin correlations, establishing a coherent ferromagnetic ordering on each aggregate. The resulting spin configuration, in which all spins on each vesicle point either outwards (o-vesicles) or inwards (i-vesicles), is the only source of cohesion for the otherwise repulsive particles of our model. The relative orientations of the spins on different aggregates determine the sign of the vesicle-vesicle interaction, whose strength, however, is very low provided

the two vesicles are outside the short range of the repulsive interactions. The second transition, taking place at $T=0.7$, leads from a liquidlike to a solidlike ordering of particles at the vesicles surface. Both transitions observed in antidipoles appear to be continuous, and are marked by broad peaks in the constant volume specific heat. The lowest temperature transition observed in antidipoles has no counterpart in the case of electrostatic dipoles.

Our simulations provide a first evaluation of the average cluster size ($\langle M\rangle=198\pm20$ at $T=0.9$, and $\langle M\rangle=168\pm20$ at $T=0$), and of the equilibrium distribution of cluster sizes, extending up to –1200 particles. We emphasize that the statistical analysis of the aggregation process is an intrinsically difficult problem, involving large scale correlations and fluctuations, as well as slow relaxation channels. In this respect, our study is admittedly a preliminary investigation of the model properties, whose quantitative results need to be confirmed and refined by longer simulation for larger samples, coupled to a detailed analysis of finite size effects and autocorrelation times.

The floating vesicles phase of antidipole provides a simple and flexible model to investigate thermal and mechanical properties of self-assembling equilibrium membranes. In this respect, our antidipoles have a close relation with the model introduced in Ref. [14]. In both cases, the stability of membranes does not require the explicit inclusion of a solvent, thus allowing the simulation of large systems [30].

A distant relation might be found also between our model and the model introduced in Ref. [31] (Widom's model) to describe amphiphile solutions. Antidipole particles, in particular, could be seen as the counterpart of surfactant molecules (AB molecules, in the notation of Ref. [31]) in Widom's model.

Despite its apparent simplicity, our model still contain several free parameters that allow to change quantitatively or even qualitatively the shape, size, and dimensionality of the equilibrium structures at low density and temperature. An example of this flexibility is provided by our investigations of finite range antidipole models, in which the spin-spin potential is smoothly terminated above a cutoff distance R_c. Upon annealing from the homogeneous fluid phase, potentials of this kind give rise to smaller vesicles for $R_c=10\sigma$, and to layered 3D structures for $R_c=3.5\sigma$. Other results might be obtained by changing the relative strength of attractive and repulsive interactions, by modifying the stiffness of the repulsive potential, or by adding an isotropic attractive tail to the particle-particle potential.

The relevance of our results and, more in general, of the antidipole model, is enhanced by the present feverish interest for nanostructures, and, in particular, for their self-organization from individual particles. These last may represent either atoms or, more frequently, larger building blocks. In the case that each of the particles in our simulation is the coarse graining representation of an organic molecule in micelles or other amphiphilic membranes, we might assume $\sigma\sim0.75$ nm, and the diameter of the largest vesicles seen in our simulations is of the order of 20σ, or ~15 nm, i.e., well into the interesting nanometric range.

We anticipate that simple additions to the basic scheme might allow the investigation of a wider range of systems and problems, including the osmotic behavior of vesicles, different vesicle-vesicle interactions, and properties of electrified membranes. Moreover, the inclusion of a kinetic energy term for the spin rotations provides a simple way of investigating dynamical properties, including elementary vibrational modes of a planar membrane or of vesicles.

[1] M. A. Miller and D. J. Wales, J. Phys. Chem. B **109**, 23109 (2005).

[2] M. J. Stevens and G. S. Grest, Phys. Rev. E **51**, 5962 (1995).

[3] A.-P. Hynninen and M. Dijkstra, Phys. Rev. E **72**, 051402 (2005).

[4] T. Tlusty and S. A. Safran, Science **290**, 1329 (2000); S. A. Safran, Nat. Mater. **2**, 71 (2003).

[5] P. I. C. Teixeira, J. M. Tavares, and M. M. Telo da Gama, J. Phys.: Condens. Matter **12**, R411 (2000).

[6] J. J. Weis and D. Levesque, Phys. Rev. Lett. **71**, 2729 (1993).

[7] M. E. van Leeuwen and B. Smit, Phys. Rev. Lett. **71**, 3991 (1993).

[8] M. S. Wertheim, J. Stat. Phys. **35**, 19 (1984).

[9] A recent discussion of the ferroelectric phase transition in dipolar hard spheres is reported in J.-J. Weis, J. Chem. Phys. **123**, 044503 (2005).

[10] S. C. Glotzer, M. J. Solomon, and N. A. Kotov, AIChE J. **50**, 2978 (2004); S. C. Glotzer, Science **306**, 419 (2004).

[11] K. Van Workum and J. F. Douglas, Phys. Rev. E **71**, 031502 (2005); J. Dudowicz, K. F. Freed, and J. F. Douglas, Phys. Rev. Lett. **92**, 045502 (2004).

[12] S. O. Nielsen, C. F. Lopez, G. Srinivas, and M. L. Klein, J. Phys.: Condens. Matter **16**, R481 (2004).

[13] G. Gompper and D. M. Kroll, *Statistical Mechanics of Membranes and Surfaces*, edited by D. R. Nelson, T. Piran, and S. Weinberg (World Scientific, Singapore, 2004) Chap. 12.

[14] J.-M. Drouffe, A. C. Maggs, and S. Leibler, Science **254**, 1353 (1991).

[15] A comprehensive description of amphiphile system properties may be obtained by complementing the results of idealized, solvent-free models (like antidipoles) with those of more detailed model, explicitly including solvent molecules. Examples of the latter are as follows: S. Yamamoto, Y. Maruyama, and S.-A. Hyodo, J. Chem. Phys. **116**, 5842 (2002); G. Srinivas, D. E. Discher, and M. L. Klein, Nano Lett. **5**, 2343 (2005).

[16] J. Zhu, Y. Jiang, H. Liang, and W. Jiang, J. Phys. Chem. B **109**, 8619 (2005).

[17] Computations for dipoles have been done with a smaller ($N=1200$) number of particles. We estimated finite size corrections by reevaluating the energy on samples of $N=9600$ particles obtained by replicating the $N=1200$ sample two times in each direction. The difference ($\delta\sim0.08\epsilon$ per atom) is smaller than the symbols' size in Fig. 2.

[18] We use the terms solidlike and glasslike in a rather empirical

way, although we are aware of the subtleties and problems concerning melting in 2D. See, for instance, K. J. Strandsburg, Rev. Mod. Phys. **60**, 161 (1988).

[19] More precisely, $du(T)/dT$ is the configurational contribution to the constant volume specific heat per particle. In addition, the constant volume specific heat includes contributions from the kinetic energy, i.e., a $1.5K_B$ term due to translational kinetic energy, and, possibly, a further term if the rotation of spins and particles adds a kinetic energy term to the Hamiltonian.

[20] The equilibration of systems with extended clustering might be enhanced by advanced MC techniques, not used in the present study. See, for instance B. Chen and J. I. Siepmann, J. Phys. Chem. B **105**, 11275 (2001).

[21] J. P. Wittmer, A. Milchev, and M. E. Cates, J. Chem. Phys. **109**, 834 (1998).

[22] Y. Rouault and A. Milchev, Phys. Rev. E **55**, 2020 (1997).

[23] B. Smit *et al.*, Langmuir **9**, 9 (1993).

[24] M. Kenward and M. D. Whitmore, J. Chem. Phys. **116**, 3455 (2002).

[25] G. J. A. Sevink and A. V. Zvelindovsky, Macromolecules **38**, 7502 (2005).

[26] R. D. Kamien, Rev. Mod. Phys. **74**, 953 (2002).

[27] C. Itzykson, in *Proceedings of the GIFT Seminar*, Jaca 85, edited by J. Abad, M. Asorey, and A. Cruz (World Scientific, Singapore, 1985), pp. 130–188.

[28] D. Espriu, Phys. Lett. B **194**, 271 (1987).

[29] C. F. Baillie, D. A. Johnston, and R. D. Williams, Nucl. Phys. B **335**, 469 (1990).

[30] Solvent-free models of amphiphilic membranes are reviewed in G. Brannigan, L. C.-L. Lin, and F. L. H. Brown, Eur. Biophys. J. **35**, 104 (2006).

[31] B. Widom, J. Chem. Phys. **84**, 6943 (1986); **81**, 1030 (1984).